Facile Construction of a Laser Scanning Optical Beam Induced Current Microscope

Ankita Buragohain, Nayan M. Kakoty, Guan-Yu Zhuo, Gazi A. Ahmed, Fu-Jen Kao, Nirmal Mazumder, and Ankur Gogoi

***Abstract*—We report on the design and construction of a laser scanning optical beam-induced current (OBIC) microscope by assembling cost-effective commercial optical and electronic hardware components and developing data acquisition and control software in LabVIEW. A preliminary OBIC image of a Si photodetector acquired by the developed microscope is presented to demonstrate its operational capability. The versatility of the design will allow for the construction of other scanning microscope modalities on the same platform.**

***Index Terms*—Current measurement, data acquisition, failure analysis, optical imaging, microscopy, semiconductor device testing.**

I. Introduction

LASER scanning optical beam-induced current (OBIC) microscopy, also known as light or laser beam-induced current (LBIC) microscopy [1], has become a powerful and non-destructive tool for high-resolution failure analysis of electronic devices [2], [3], [4]. The principle of OBIC lies in the generation of electron-hole pairs when a laser beam of suitable energy is focused and scanned on the semiconductor sample in a raster fashion. The synchronized detection of the resultant current profile with respect to the beam positions allows the subsequent generation of contrast images of the active regions within the device. This, in turn, allows for the visualization of structural defects, monitoring of the photoresponse and device performance and studying electrical properties such as the carrier lifetime and diffusion length [5]. Notably, OBIC microscopes are generally constructed by integrating appropriate electronics into a commercial confocal laser scanning microscope (CLSM). However, such systems are too expensive to be afforded by many laboratories [6]. In this context, several groups have reported the development of cost-effective CLSMs for various microscopy applications [7], [8], [9]. It is worth noting that these advancements primarily concentrated on biological imaging and were not specifically optimized for applications related to OBIC and/or other types of semiconductor device characterization. In contrast, K. G. Anand designed an LBIC microscope that used fixed laser beam and an XY translation stage for scanning to study semiconductor samples, including solar cells and epitaxial layers [10]. Nonetheless, these traditional stage scanning methods typically result in slower imaging speeds compared to laser scanning based on galvo mirrors [11].

In this work, we report the design and fabrication of a cost-effective laser scanning OBIC microscopy system by assembling the multispectral laser source, galvanometer mirror scanning unit, (scan and tube) lens assembly, inverted microscope, and data acquisition unit. Notably, galvanometer mirror-based laser scanning microscopes offer better resolution than traditional charge-coupled device (CCD) based or XY scanning stage-based techniques [12]. LabVIEW software was used for data acquisition and image reconstruction. The design considerations and preliminary measurements are presented in the following sections.

II. Optomechatronic Design of the OBIC Microscope

The experimental scheme of the microscope OBIC microscope is depicted in Fig. 1. A laser beam with a wavelength of 638 nm from a multispectral laser source is directed through shutter S and mirrors M1 and M2 to the large beam (10 mm) diameter scanning XY galvanometer mirror system (GVS012, Thorlabs), consisting of two galvanometer motors and two scan mirrors mounted at the end of the actuators. Each of these galvanometer motors has position detectors that provide information on the positions of the mirrors. The motor's acceleration is directly proportional to the current applied to it and provides the characteristics of a fast response. The X-Y mirror assembly is

Manuscript received 19 October 2023; revised 19 December 2023; accepted 31 December 2023. Date of publication 4 January 2024; date of current version 26 January 2024. The work of Ankur Gogoi was supported by the Science and Engineering Research Board, Department of Science and Technology (DST), India, under Grant CRG/2019/004868. The work of Nayan M. Kakoty was supported by IHFC, DST, Government of India, India, under Grant GP/2021/RR/017. This work was supported in part by the Global Innovation and Technology Alliance, Department of Science and Technology, India, under Project GITA/DST/TWN/P-95/2021, Government of India, India. *(Corresponding authors: Nirmal Mazumder; Ankur Gogoi.)*

Ankita Buragohain and Nayan M. Kakoty are with the Embedded Systems and Robotics Lab, School of Engineering, Tezpur University, Tezpur, Assam 784028, India (e-mail: ankitapburagohain93@gmail.com; nkakoty@tezu.ernet.in).

Guan-Yu Zhuo is with the Institute of Translational Medicine and New Drug Development, China Medical University, Taichung 40402, Taiwan (e-mail: zhuo0929@mail.cmu.edu.tw).

Gazi A. Ahmed is with the Department of Physics, Tezpur University, Tezpur, Assam 784028, India (e-mail: gazi@tezu.ernet.in).

Fu-Jen Kao is with the Institute of Biophotonics, National Yang-Ming Chiao Tung University, Taipei 11221, Taiwan (e-mail: fjkao@ym.edu.tw).

Nirmal Mazumder is with the Department of Biophysics, Manipal School of Life Sciences, Manipal Academy of Higher Education, Manipal, Karnataka 576104, India (e-mail: nirmal.mazumder@manipal.edu).

Ankur Gogoi is with the Department of Physics, Jagannath Barooah College, Jorhat, Assam 785001, India (e-mail: ankurgogoi@gmail.com).

This article has supplementary downloadable material available at https://doi.org/10.1109/JPHOT.2024.3349930, provided by the authors.

Digital Object Identifier 10.1109/JPHOT.2024.3349930

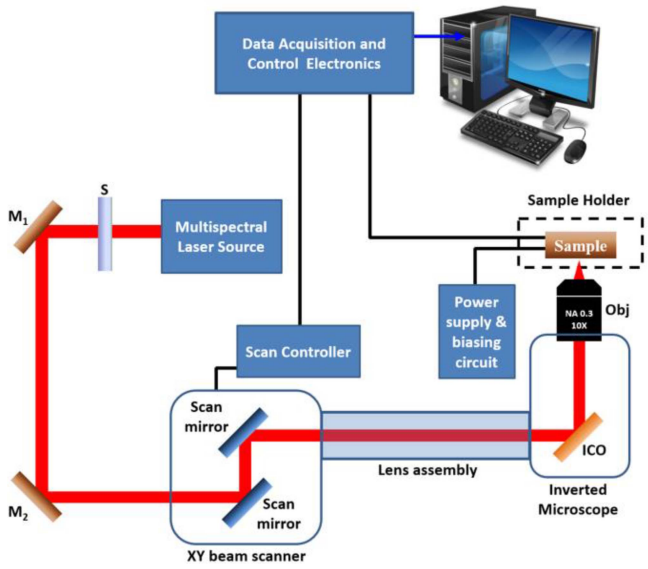

Fig. 1. Experimental setup. S: Shutter, M1, M2: Mirror; C: Obj: Objective lens, ICO: Infinity corrected optics. Black lines represent electrical interconnections.

driven by tuning with two driver circuit boards. It uses signals from the position detector to drive the actuators to the demanded position by using the positional error, speed, and integral of current terms. It consists of a proportional derivative circuit that helps to achieve better performance of the actuators. Notably, the control signals for the scan driver circuits are provided by two analog output channels of a high-speed multifunctional input-output (data acquisition and control) device (National Instruments PCIe 6351) [13], which also serves as the data acquisition system by acquiring the measured photocurrent through two analog input channels for computer interfacing. It requires -10 V to $+10$ V analog output voltage to drive both the X and Y galvanometer mirror scanners, which are differential. Sampling frequencies higher than 10 kS/s are required with a minimum number of samples equal to 1000. The signals from the PCIe 6351 device are coupled to the galvanometer driver circuit boards through the SCB-68A noise rejecting shielded I/O connector block having 68 input-output analog and digital terminals and an SCH68-68-EPM shielded connecting cable.

The laser beam, after passing through the galvo scanner, is focused on the conjugate plane of the microscope by using a scan lens (LSM02-VIS, Thorlabs). The scanning laser spot is relayed through the infinity corrected optics of the inverted microscope (HO-AMS-FL5000, Holmarc Opto-Mechatronics, India) and ultimately focused by a 10X microscope objective (HO-PA-MO10X, Holmarc Opto-Mechatronics, India) on the semiconductor sample placed on a computer-controlled XYZ positioner of an inverted microscope. The induced photocurrent is collected as a function of the beam positions in terms of the XY scanning coordinates, and an OBIC map (two-dimensional spatially resolved map) is obtained by raster scanning the laser beam on the active area of the device under test (DUT). The scan controller and data acquisition software were programmed in LabVIEW [14] and are described in the next section. After data collection, the OBIC map can be visualized in the graphical user interface (GUI) of the software, which can further be exported as an array to an Excel file for subsequent processing and generating 3D projections of the OBIC map. The aggregate cost of the components employed in building this microscope is projected to be $15000, a considerable contrast to the approximate $100000 price range associated with commercial confocal microscopes [15]. More specific information on the primary components utilized in the construction, along with their respective costs, can be found in supplementary information (Sup. Table 1).

III. Software Interface Development

Software with a GUI was developed in LabVIEW for the control of the XY galvanometer mirror scanners. The present program is based on the LabVIEW programs reported by Ferrand [16] and Zengin [17], which is optimized for the present study by adding improved features. The current software features both unidirectional (where the Y position updates only after the X position returns to its original position at the end of one cycle) and bidirectional (where the Y position updates whenever the X position reaches its maximum or minimum value) raster patterns. Importantly, each of these scanning mechanisms has its own advantages and disadvantages, and the introduction of this functionality aims to enhance flexibility in the scanning process [11], [18]. Additionally, the software includes features such as ‘Error Out’ and ‘Task Out’ to gather information about any errors that may arise during software execution and to ensure the successful completion of input tasks using the command signal, respectively. Moreover, functionality for visualizing the acquired data has been integrated into the software.

Notably, the entire LabVIEW program has been built using three subprograms. Each subprogram has its purpose, starting from initializing the system by configuring analog output and input channels with proper synchronization to deliver and measure voltages at a certain scan speed. The scanning process is performed for the entire frame over the sample area by creating a 2D raster pattern waveform based on the scanning parameters, e.g., the number of pixels in the X and Y axes, the scanning amplitude of the X and Y axes, etc. The generated analog output command signals are sent to the drivers of the mirror scanners along with the analog input data acquisition, which starts in synchronization with the command signal.

Fig. 2 shows the front panel of the LabVIEW program. The desired scanning pattern, i.e., single direction (uniform), single direction (fast reset), and bidirectional, can be selected in the designated drop-down menu in ‘Creation of Various Raster Pattern’ section. In the same section, the user can reset the Y mirror position, set the number of pixels or points to be given along the X and Y dimensions, and set the maximum and minimum values of the voltage signals sent to the X and Y mirrors. The ‘Signal Generation’ section allows for the setting of desired pixel dwell time, selection of the start trigger terminal, analog output channels, and the minimum and maximum analog output and input voltages to be applied through the data acquisition and control device. The user can stop the scanning process, if desired, by using the ‘QUIT’ button placed in the top left corner. The

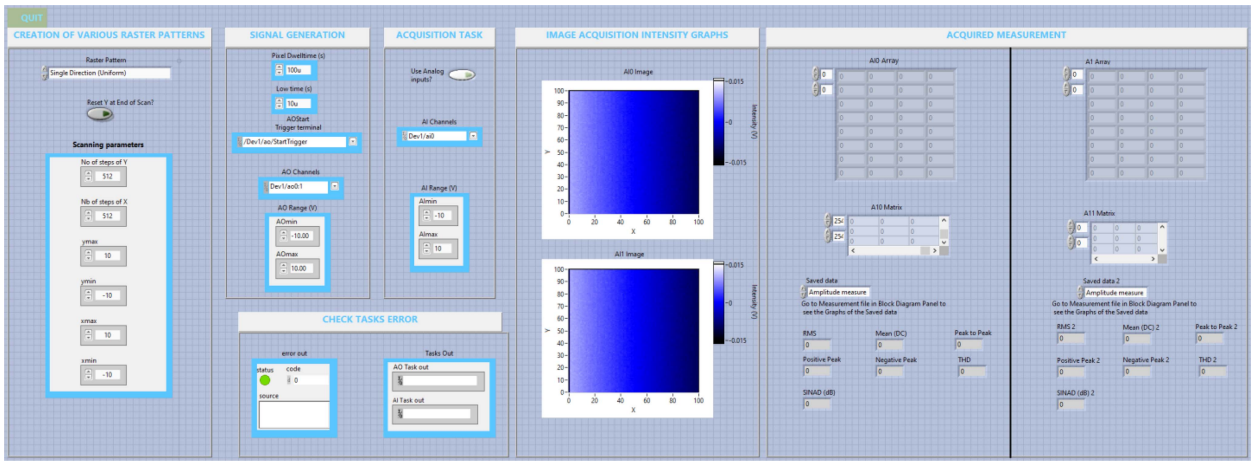

Fig. 2. Graphical user interface (front panel) of the LabVIEW program "Galvano_Mainprogram.vi".

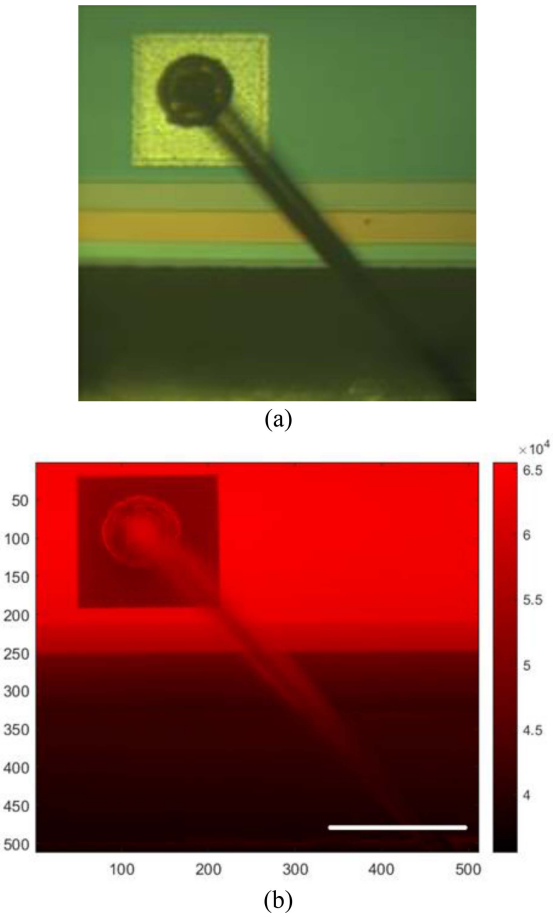

Fig. 3. (a) Reflected image of the ROI and (b) OBIC image of the ROI reconstructed in the LabVIEW software. The scale bar is 0.2 mm. The scale bar is 0.2 mm. The color bar accompanying the OBIC images signifies photocurrent intensity in arbitrary units, utilizing the entire 16-bit resolution (ideal dynamic range: 0-65535) of the A/D converter integrated into the scanning platform.

software is capable of acquiring data from all 8 differential or 16 single-ended analog input channels of the NI PCIe 6351 I/O device, which is an important feature for multimodal laser scanning microscopy applications. Notably, various alternative optical imaging techniques are available for the characterization of semiconductor devices, including methods such as polarization-resolved electroluminescence [19], optical beam-induced resistance change (OBIRCH) [20], near-infrared (NIR) thermoreflectance [21], thermal imaging based on temperature-dependent two-photon fluorescence (TPF) [22], etc. These techniques can be seamlessly integrated into the current microscope design for applications involving correlative or colocalization microscopy, achieved by adding suitable electronic or optical components. Furthermore, the multichannel data acquisition capability enables the integration of other imaging methods, such as four-channel Stokes polarimetry, fluorescence anisotropy imaging, etc. [23], [24], [25]. The desired analog input channels and the input voltage range can be selected in 'Acquisition Task' section. Notably, the present version of the software is restricted to display only two images from two analog input channels, as seen in the 'Image Acquisition Intensity Graphs' section, which can be easily increased, if needed. On the other hand, the 'Acquired Measurement' section can be used to visualize the acquired data. The 'Error Out' and the 'Task out' are located in 'Check Tasks Error' section. The flowchart of the software can be found in the supplementary information (Sup. Fig. 1).

IV. Preliminary Results

After optical alignment, the microscope was used to image the active area of a Si PIN photodiode (BPW34) at an incident wavelength of 638 nm. Notably, many researchers have used this photodiode as a mini solar cell in the recent past [26], [27]. For this work, the photodiode was used in photovoltaic (zero-bias) mode, which can be easily subjected to reverse bias (photoconductive mode) as well, enabling the measurement of higher powers with increased speeds. In both operational modes, the magnitude of the photocurrent corresponds directly to the intensity of the light that is incident upon the photodiode. The samples were scanned at a rate of 31.45 sec/frame (120 μs pixel dwell time) at 512 $\times$ 512 pixels. A 20X (numerical aperture

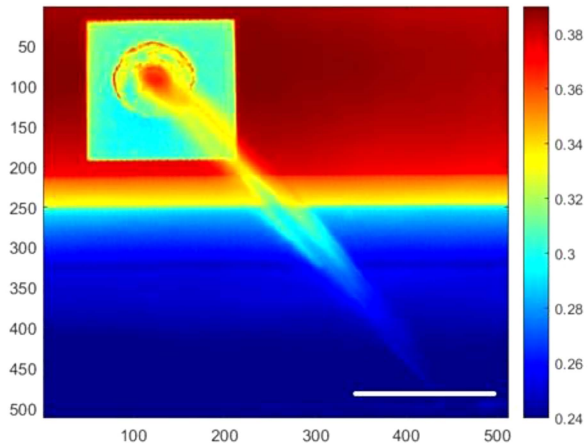

Fig. 4. Image of internal quantum efficiency (IQE) reconstructed from OBIC measurements. The scale bar is 0.2 mm.

$= 0.40$) objective lens is employed for image acquisition. For this objective, the full width at half maximum spot size is found to be 1.22 μm. At the focal point, the average power measured was found to be $\sim$116 μW; therefore, the average energy exerted on the specimen for each pixel is approximately 0.014 μJ (obtained by 120 μs $\times$ 116 μW). The scan area was approximately 1100 μm $\times$ 1100 μm.

Fig. 3(a) shows the reflected widefield image of the region of interest (ROI) of the photodiode acquired by using the same objective through the secondary camera port of the microscope. In Fig. 3(b), the OBIC image of the ROI is presented, reconstructed in MATLAB using the acquired data exported from LabVIEW. Alternatively, image reconstruction can be performed using other software or computer code developed in Python, Scilab, etc. The image is color coded according to the incident wavelength (red, 638 nm). In these OBIC images, the reconstructed region of the active area of the photodiode appears uniform indicating that the area is homogeneous. In these OBIC images, one can also observe the significantly diminished current intensity in the regions that are not photosensitive including the anode region and the region below the active region. The observed sharp edges of both the anode and active areas ensure that defocus did not occur during the laser scanning.

We further demonstrate the determination of the internal quantum efficiency (IQE) from the spatially resolved OBIC signals by adopting the models used by several other researchers [28], [29]. Notably, IQE refers to the efficacy with which photons, avoiding loss through reflection or transmission, can generate charge carriers that are viable for collection. Fig. 4 shows the spatially resolved IQE of the ROI studied by OBIC microscopy.

V. Conclusion

OBIC measurements on semiconductor devices carry a lot of information by which electrically active defects and localized inhomogeneities can be classified and even identified, which helps to better understand the charge transfer process and failure mechanism in such devices. In this letter, the facile assembly of a laser-scanning OBIC microscope is demonstrated. In contrast to commercial systems that are not easily modifiable, the present setup proposed here allows for optimization and configuration tailored to specific multimodal microscopy applications. Additionally, the multispectral laser source with emission wavelengths at 445 nm, 520 nm, and 638 nm will allow for spectrally resolved OBIC measurements.

Preliminary results ensured the operational capability of the microscope in acquiring OBIC images from semiconductor samples. The performance of the microscope including the signal-to-noise ratio of the measurements can be further improved by using appropriate signal amplifier, filter, and intensity-modulated light sources coupled with lock-in detection. Notably, the results obtained from such studies will certainly help to understand the correlation between material defect and the failure modes associated with solar cells, LEDs, and other electronic devices and to further improve their performance and reliability.

Acknowledgment

The authors would like to thank the Indian Science Technology and Engineering facilities Map (I-STEM), a Program supported by Office of the Principal Scientific Adviser to the Government of India, for enabling access to the MATLAB software suite used to carry out this work.

References

[1] M. Boostandoost, *Signature of Photon Emission and Laser Stimulation for Failure Analysis of Semiconductor Devices With Respect to Thin-Film Solar Cells*. Berlin, Germany: Technische Universität Berlin, 2013.

[2] C. Xu and W. Denk, "Comparison of one-and two-photon optical beam-induced current imaging," *J. Appl. Phys.*, vol. 86, no. 4, pp. 2226–2231, 1999.

[3] E. Esposito, F. Kao, and G. McConnell, "Confocal optical beam induced current microscopy of light-emitting diodes with a white-light supercontinuum source," *Appl. Phys. B*, vol. 88, no. 4, pp. 551–555, 2007.

[4] G. Zhuo et al., "An insight into optical beam induced current microscopy: Concepts and applications," *Microsc. Res. Techn.*, vol. 85, no. 11, pp. 3495–3513, 2022.

[5] R. Hristu, S. Stanciu, S. Wu, F. Kao, O. Kwon, and G. Stanciu, "Optical beam induced current microscopy of photonic quantum ring lasers," *Appl. Phys. B*, vol. 103, no. 3, pp. 653–657, 2011.

[6] A. Halpern, M. Lee, M. Howard, M. Woodworth, P. Nicovich, and J. Vaughan, "Versatile, do-it-yourself, low-cost spinning disk confocal microscope," *Biomed. Opt. Exp.*, vol. 13, no. 2, pp. 1102–1120, 2022.

[7] P. Xi, B. Rajwa, J. Jones, and J. Robinson, "The design and construction of a cost-efficient confocal laser scanning microscope," *Amer. J. Phys.*, vol. 75, no. 3, pp. 203–207, 2007.

[8] N. Callamaras and I. Parker, "Construction of a confocal microscope for real-time xy and xz imaging," *Cell Calcium*, vol. 26, no. 6, pp. 271–279, 1999.

[9] S. Arunkarthick, M. Bijeesh, A. Vetcha, N. Rastogi, P. Nandakumar, and G. Varier, "Design and construction of a confocal laser scanning microscope for biomolecular imaging," *Curr. Sci.*, vol. 107, no. 12, pp. 1965–1969, 2014.

[10] K. Anand, "Laser beam induced current (LBIC) instrumentation for semiconductor research," *Int. J. Eng. Manage. Sci.*, vol. 4, no. 2, pp. 102–107, 2013.

[11] P. Xi, Y. Liu, and Q. Ren, "Scanning and image reconstruction techniques in confocal laser scanning microscopy," in *Laser Scanning, Theory and Applications*. London, U.K.: IntechOpen, 2011, pp. 523–544.

[12] S. Hong et al., "Confocal scanning electroluminescence spectro-microscope for multidimensional light-emitting property analysis," in *Gallium Nitride Materials and Devices II*, vol. 6473. Bellingham, WA, USA: SPIE, 2007, pp. 461–466.

[13] National Instruments, "PCIe-6351 and USB-6351 specifications," 2023. Accessed: Feb. 3, 2023. [Online]. Available: https://www.ni.com/docs/en-US/bundle/pcie-usb-6351-specs/page/specs.html
[14] National Instruments, "LabVIEW," 2023. Accessed: Feb. 3, 2023. [Online]. Available: https://www.ni.com/en-in/shop/software/products/labview.html
[15] Fogarty International Center Available, "Focus on mobile health: Innovative microscope enables early cancer diagnoses," 2023. Accessed: Dec. 17, 2023. [Online]. Available: https://www.fic.nih.gov/News/GlobalHealthMatters/january-february-2020/Pages/mobile-health-innovative-microscope-enables-early-cancer-diagnoses.aspx
[16] P. Ferrand, "GPScan. VI: A general-purpose LabVIEW program for scanning imaging or any application requiring synchronous analog voltage generation and data acquisition," *Comput. Phys. Commun.*, vol. 192, pp. 342–347, 2015.
[17] B. Zengin, "Instrumentation of an opto-digital confocal microscope and development of a DMD-based imaging setup," M.S. thesis, Koç Univ., Istanbul, Turkey, 2018.
[18] National Instruments, "Generate 2D raster pattern in LabVIEW," 2023. Accessed: Dec. 17, 2023. [Online]. Available: https://forums.ni.com/t5/Example-Code/Generate-2D-Raster-Pattern-in-LabVIEW/ta-p/3503399
[19] F. Peters and D. Cassidy, "Spatially and polarization resolved electroluminescence of 1.3-μm InGaAsP semiconductor diode lasers," *Appl. Opt.*, vol. 28, no. 17, pp. 3744–3750, 1989.
[20] K. Nikawa, C. Matsumoto, and S. Inoue, "Novel method for defect detection in Al stripes by means of laser beam heating and detection of changes in electrical resistance," *Japanese J. Appl. Phys.*, vol. 34, no. 5R, 1995, Art. no. 2260.
[21] G. Tessier, M. Bardoux, C. Filloy, C. Boué, and D. Fournier, "High resolution thermal imaging inside integrated circuits," *Sensor Rev.*, vol. 27, no. 4, pp. 291–297, 2007.
[22] G. Zhuo, H. Su, H. Wang, and M. Chan, "In situ high-resolution thermal microscopy on integrated circuits," *Opt. Exp.*, vol. 25, no. 18, pp. 21548–21558, 2017.
[23] N. Mazumder et al., "Polarization-resolved second harmonic generation microscopy with a four-channel Stokes-polarimeter," *Opt. Exp.*, vol. 20, no. 13, pp. 14090–14099, 2012.
[24] N. Mazumder et al., "Label-free non-linear multimodal optical microscopy—Basics, development, and applications," *Front. Phys.*, vol. 7, 2019, Art. no. 170.
[25] K. Suhling, J. Levitt, and P. Chung, "Time-resolved fluorescence anisotropy imaging," in *Fluorescence Spectroscopy and Microscopy Methods in Molecular Biology*, vol. 1076. Totowa, NJ, USA: Humana Press, 2014, pp. 503–519.
[26] I. Bubli et al., "Enhancement of solar cell efficiency via luminescent downshifting by an optimized coverglass," *Ceram. Int.*, vol. 46, no. 2, pp. 2110–2115, 2020.
[27] L. Florêncio, L. Gómez-Malagón, B. Lima, A. Gomes, J. Garcia, and L. Kassab, "Efficiency enhancement in solar cells using photon down-conversion in Tb/Yb-doped tellurite glass," *Sol. Energy Mater. Sol. Cells*, vol. 157, pp. 468–475, 2016.
[28] D. Sontag, G. Hahn, P. Geiger, P. Fath, and E. Bucher, "Two-dimensional resolution of minority carrier diffusion constants in different silicon materials," *Sol. Energy Mater. Sol. Cells*, vol. 72, no. 1-4, pp. 533–539, 2002.
[29] B. Moralejo et al., "LBIC and reflectance mapping of multicrystalline Si solar cells," *J. Electron. Mater.*, vol. 39, pp. 663–670, 2010.